Microsystem Technologies 10 (2004) 472–477 © Springer-Verlag 2004
DOI 10.1007/s00542-004-0375-6

Effect of workpiece springback on micromilling forces

C. R. Friedrich, V. P. Kulkarni

Abstract The machining forces present in micromilling with tools in the 50–100 μm diameter range are dominated by contact pressure and friction between the tool cutting edges and the workpiece. A model of the micromilling process was developed based on the elastic contact between the tool and the workpiece along the side and bottom cutting edges of the tool. Micromilling experiments were conducted on 6061-T6 aluminum to obtain machining forces in the feed and cross-feed directions during slot milling and partial engagement end milling. Comparisons with the experimental data indicate reasonable agreement for full slot milling as well as end milling with radial depths of cut in the range of 2 μm to 40 μm. It was concluded that this model is adequate for predicting micromilling forces with the precision needed to reduce tool breakage and workpiece clamping forces and for predicting tool deflection that affects wall slope and feature size.

1 Introduction

Milling is a versatile process at conventional sizes and at the microscale. A drawback is the slow material removal rates that limit productivity and add cost to the machined parts. However, for prototyping and the fabrication of replication masters, particularly for microfluidic applications, micromilling can economically compete with other processes. Microscale cutting forces must be reduced to acceptable levels that will ensure long tool life yet reasonable removal rates. The ability to quickly predict the machining forces dominated by parasitic contact forces is necessary for better process planning. Knowing the forces present during micromilling can help reduce or eliminate tool breakage. Tool changeout represents not only a loss of productivity but also a loss of precision due to variations in the basic dimensions of the tools, variation in the length extending from the collet, and variable runout in the collet. The purpose of the present study was to develop a model for predicting micromilling forces with relatively little input other than two material properties and the cutting edge radii of the micromilling tools. This micromilling model is based solely on the elastic interaction between the tool and the work material and is adopted from a predictive model for precision diamond machining.

Waldorf, et al. [1] developed a model based on a slip line field for orthogonal cutting at large negative rake angles in turning and using aluminum 6061-T6 they concluded that larger cutting edge radii give larger ploughing forces. Bao and Tansel [2–4] studied the micromilling process using 700 μm diameter high-speed steel and carbide milling tools on aluminum, steel, and copper. The model was based on the assumption that the tangential cutting force is proportional to the uncut chip area and the radial cutting force is proportional to the tangential cutting force and on the trochoidal nature of the tool path. Several studies have been conducted on single point diamond machining by Moriwaki and Okuda [5] and Furukawa and Moronuki [6] using the specific cutting energy approach for diamond machining. These investigators found that as the ratio of the uncut chip thickness to the radius of the cutting edge was reduced, the specific cutting energy increased exponentially to approximately 100-times that at conventional sizes. Arcona and Dow [7] developed a cutting force model for diamond machining based on elastic contact and friction between the tool and an Al 6061-T6 workpiece, among other materials. While the model also included shearing forces for a very sharp and rigid tool, the results showed that as the uncut chip thickness was reduced the contribution by shearing to the total cutting forces greatly reduced while the elastic contact and friction components approached an assymptotic level. These parasitic forces were attributed to elastic springback of the workpiece as it is compressed and moved under the cutting edge without being removed. The model required the hardness and elastic modulus of the workpiece and two empirical constants were obtained from cutting measurements.

2 Micromilling model development

The model developed by Arcona and Dow for diamond machining, based on workpiece elastic springback, was

Received: 8 August 2003 / Accepted: 6 November 2003

C. R. Friedrich (✉)
Department of Mechanical Engineering, Engineering Mechanics, Michigan Technological University, Houghton, MI 49931, USA
e-mail: craig@mtu.edu

V. P. Kulkarni
Norman Noble, Inc., Cleveland, Ohio, USA

This work was supported primarily by the Engineering Research Centers Program of the National Science Foundation under Award Number EEC-9986866. The Engineering Research Center for Wireless Integrated Microsystems is also hereby acknowledged. All machining was performed at the Micromechanical Applications and Processes Laboratory at Michigan Technological University.

modified for the very different cutting environment of micromilling. The model requires only two material properties of the workpiece and the cutting edge geometry of the tool being used. It is therefore straightforward and easily adaptable for cutting force prediction under production conditions. It is made more difficult, however, by the much more complex geometry of micromilling tools.

2.1 General micromilling force equations

The basic assumption of the micromilling model is that for micromilling tools in the range of 50–100 μm and an uncut chip thickness in the sub-micrometer range, the machining forces are dominated by elastic normal contact and sliding friction between the workpiece and the edges of the micromilling tool as shown in Fig. 1. The figure shows one of the cutting edges of a micromilling tool. A two-fluted tool has two bottom cutting edges as well as two side cutting edges, each with four resultant force components that are fixed relative to the rotating tool but variable relative to a stationary workpiece or force dynamometer. The magnitude and angle of each resultant depends on the radius of the cutting edge, the flank angle, and the springback depth, which is a function of workpiece hardness and elastic modulus and the cutting edge radius.

The major differences between the Arcona and Dow model and the proposed micromilling model are that the milling tool edge radii are on the order of several micrometers, the milling tool has a variable uncut chip thickness, and the milling tool has multiple edges in contact with the workpiece with time-varying force resultants at any instant of tool rotation. On any cutting edge of the micromilling tool, the local forces in the cutting and thrust directions are given by,

$$F_c = F_s \cos\phi + F_n \sin\phi + F_{c\_\text{elastic}}$$
$$F_t = \mu \cdot (F_c - F_{c\_\text{elastic}}) + F_{t\_\text{elastic}} \quad (1)$$

where the elastic force resultants depend on the compression of the workpiece (springback) and the sliding friction, and are a function of the contact area between the edges and the workpiece. These terms will be subsequently broken into individual components. The remaining terms represent the commonly used normal and tangential forces on the shear plane. The springback in the micromilling process is represented as a linear function of tool edge radius and the ratio of material hardness to elastic modulus. The springback (s) and the normal contact stress (σ_f) are given by,

$$s = k_1 r \frac{H}{E}$$
$$\sigma_f = k_2 H \sqrt{\frac{H}{E}} \quad (2)$$

where $k_1 = 43$ and $k_2 = 4.1$ and were experimentally obtained as a best-fit for several materials including 6061-T6 aluminum [7]. The value of the springback and the tool edge radius determine the area of contact between the tool and workpiece as well as the orientation of the resultant of this force with respect to a tool coordinate system. Therefore, the final local cutting and thrust forces on any edge are given by,

$$\text{Cutting Force } F_c = \frac{HA_c}{3}\left(\frac{\cot\phi}{\sqrt{3}} + 1\right) + \mu_f A_f \left((4.1.H)\sqrt{\frac{H}{E}}\right)$$
$$\text{Thrust Force } F_t = \mu\left[\frac{HA_c}{3}\left(\frac{\cot\phi}{\sqrt{3}} + 1\right)\right] + A_f\left((4.1.H)\sqrt{\frac{H}{E}}\right) \quad (3)$$

where the cutting direction is the local relative velocity between the tool edge and the workpiece and the thrust direction is perpendicular. The second term in each equation is the force due to springback and is the focus of the remainder of this investigation. For the micromilling regime where chip areas are often a fraction of a square micrometer the first terms of Eq. 3 are relatively insignificant. This largely explains the so called size effect where the measured machining forces approach a constant value as the uncut chip thickness approaches zero.

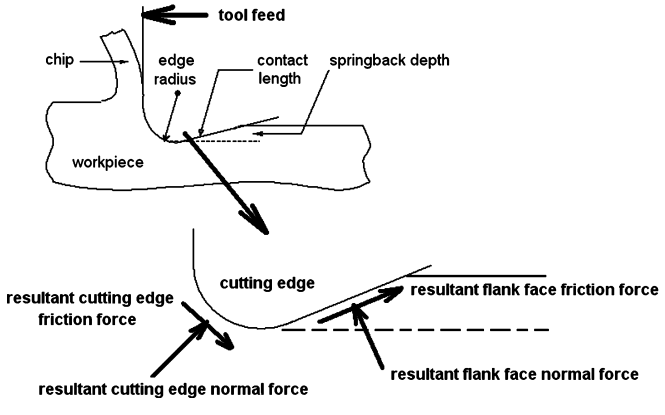

Fig. 1. Generalized micromilling tool cutting edge and flank with resultant normal contact forces and friction forces. Magnitude and orientation of resultant force vectors depend on tool geometry and work piece springback depth

2.2 Forces on specific tool edge

Commercial micromilling tools with a diameter less than 127.5 μm (0.005") are available as two fluted, spade-type tools with bottom cutting edges, side cutting edges, and side taper as shown in Fig. 2. The tool can be in contact with the workpiece at six different areas namely the bottom cutting edge, bottom rake face, bottom flank face, side cutting edge, side rake face, and side flank face. At each of these six locations there will be both normal and friction forces due to elastic springback. The process of predicting the total springback-based forces is to first determine the depth of the springback (s) and contact pressure (σ_f) from Eq. (2). Based on this depth and the geometry of the various tool edges, the contact area and thus the normal contact force and friction force on each edge were calculated. Then the resultant normal force and friction force vectors are calculated and summed. The resultants are

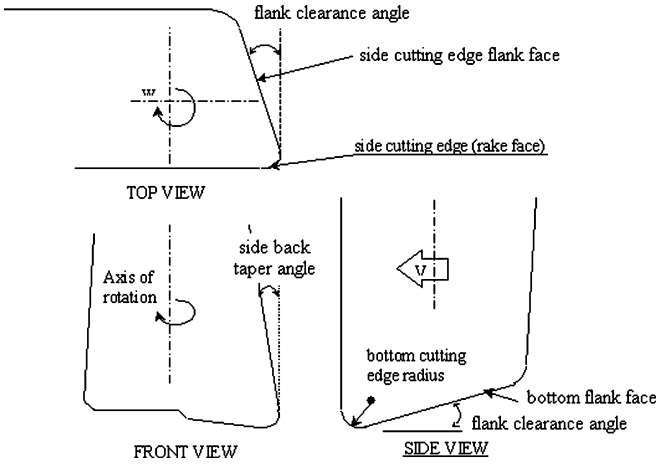

Fig. 2. Orthographic views of two-fluted micromilling tool showing multiple bottom and side cutting edges and taper and clearance angles

resolved into tool-based coordinates in the tool radial, tangential, and axial directions. Values of these forces for varying milling tests will be subsequently shown in the comparisons between the model and experiments.

For the commercial micromilling tools used, the various angles and edge radii are given in Table 1 and a micrograph of the tool is shown in Fig. 3. The micrograph is from a white-light interferometric microscope whereby the bottom and side cutting edge radii and relief angles were quantified.

Table 1. Geometry of new 100 μm diameter micromilling tool

Tool material	Tungsten Carbide
Average side cutting edge radius	2 μm (standard deviation 0.8 μm)
Average bottom cutting edge radius	2 μm (standard deviation 0.9 μm)
Side flank relief angle	15°
Bottom flank relief angle	17°
Tool back taper	1.5°

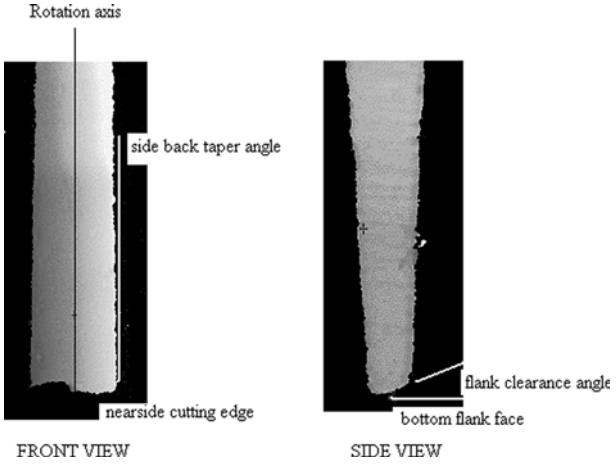

Fig. 3. White-light interferometric micrographs from which milling tool topography was extracted to determine edge radii and angles

2 Experimental procedure

In addition to the machining parameters and material properties, the geometric variables of the micromilling tool must be determined. The variables required for the model are the side and bottom cutting edge radii and the flank clearance angles. To determine these values, several 100 μm diameter tungsten carbide tools, later used in cutting tests, were examined under a white-light interferometric microscope. These measurements gave the edge radii and flank angles shown in Table 1. The edge radii were measured along the bottom and side cutting edges and the average value of 2 μm was used for all subsequent calculations. The springback depth is a linear function of the edge radii and the contact lengths were assumed to be a linear function of the flank angles. With small variations in the angles, this is a reasonable assumption.

To measure the cutting forces, a two-axis dynamometer was built using long time constant piezoelectric force sensors. Each axis was calibrated using dead weights in the force range between 10 and 100 mN and the calibration was linear with a sensitivity of approximately 3 mN/mV. During machining tests, the sensor output was stored in a digital recording oscilloscope at a sampling frequency of 20 kHz and later downloaded for conversion to force levels and subsequent analysis. The machining parameters are shown in Table 2.

The two-fluted milling tools were placed in the spindle collet of a custom high precision micromilling machine and the radial runout was measured with an air-bearing linear variable differential transformer. With no special centering effort, the radial runout was measured to be 5.5 μm. Instead of attempting to true the tool in the spindle, it was decided to leave the tool with runout. This resulted in the tool cutting with only one side cutting edge and made interpretation of the force signals easier than if the signal had contained simultaneous data from both side cutting edges.

3 Data and results

A typical dynamometer output seen on the oscilloscope for a 100 μm diameter milling tool at 10 μm/sec feedrate and 8000 rpm while cutting a full slot is shown in Fig. 4. The data sampling rate was 20 kHz. The purpose of the study was to predict and measure the maximum milling forces in the feed and cross-feed directions rather than to study the dynamic behavior of the process. Therefore, to reduce the computational burden the stored data was

Table 2. Material properties and machining parameters for micromilling tests

Spindle speed	8,000 rpm
Feedrate	5, 10, 20 μm/sec
Axial depth of cut	5, 10, 15 μm
Radial depth of cut	2, 5, 10, 20, 40, 100 μm
6061-T6 Aluminum elastic modulus	69 Gpa [7]
6061-T6 Aluminum vickers hardness	1 Gpa [7]
Calculated springback depth	1.24 μm

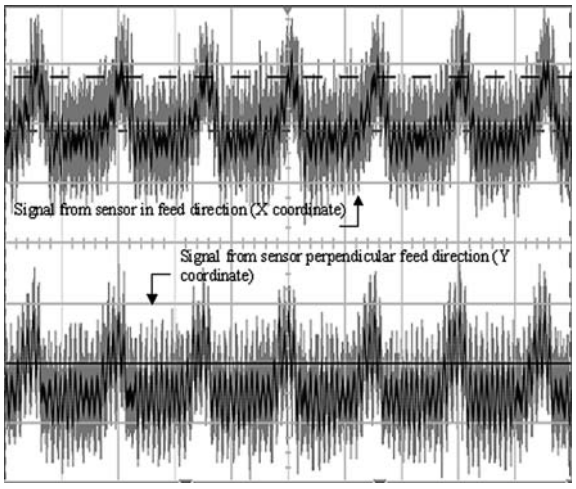

Fig. 4. Typical force signals from two-axis dynamometer force sensors for full slot milling with 100-micron diameter tool. Upper trace is in the work piece feed direction and the lower perpendicular to it

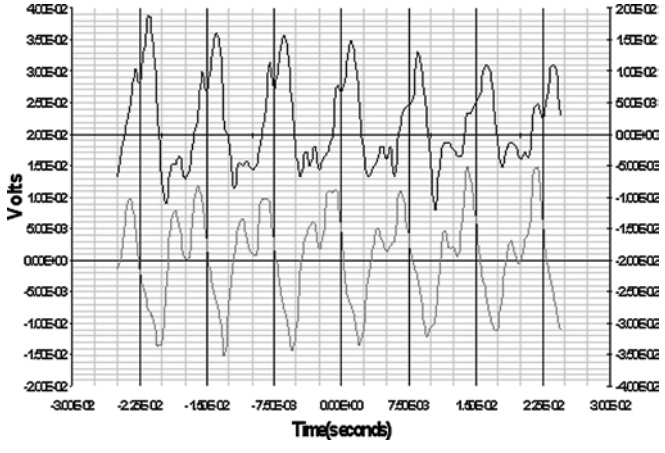

Fig. 5. Data for 100-micron slot milling after applying a 2 kHz low pass filter. Each major time axis division (vertical) is 7.5 ms and each major voltage axis division (horizontal) is 16 mN. Trace is from one cutting edge with the tool rotating at 8,000 revolutions per minute

sampled at every tenth data point, acting as a 2 kHz low pass filter, and entered into a spreadsheet program for analysis and plotting. Two such plots are shown in Fig. 5, which is from full slot milling. The upper trace is in the work piece feed direction and the lower trace is perpendicular to the feed direction, in the radial direction of the uncut material. The longer contact time between the edges and the work is easily seen as well as occasional double peaks in the feed direction. These double peaks were not expected however the model does predict them.

The full slot feed direction data was analyzed for signal content to identify features of the signal because at small radial depths of cut, shown later, the signal to noise ratio drops making it more difficult to identify details. This comparison was also performed to determine how well the model predicted the force dynamics even though this was not a focus of this study. A comparison between the model and one rotation of the tool (from Fig. 5) is shown in

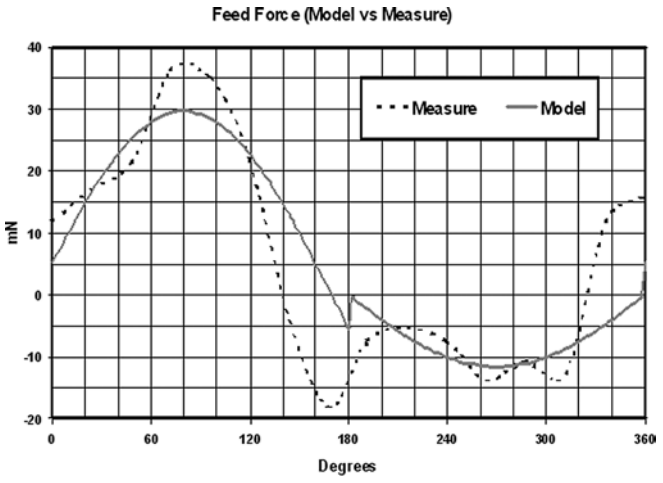

Fig. 6. Comparison of predicted and measured force data for one revolution of the 100-micron diameter tool with one side cutting edge and both bottom cutting edges contacting in full slot milling

Fig. 6. Here, zero-degrees represents that the side cutting edge rake face is perpendicular to the feed direction. Because the tool has a parallelogram shape and the dimensions of the tool are large compared to the feed per revolution, this angle is different than the angle defined by the center of rotation of the tool and the radius of the side cutting edge. The locations of the force peaks and their magnitude are in good agreement as well as the shape of the force curves. There appears to be noise in the measured data, which is to be expected. Therefore, the model generally tends to smoothen the force data but provides adequate agreement to apply the model to small radial depths of cut. The discontinuity at 180° in the model line is where the side cutting edge instantly leaves the workpiece and that component of the force vanishes. In reality, this feature would be smoothened due to chip breakage and the finite size of the cutting edge and this is present in the measured data line. The discontinuity at 360° is due to the side cutting edge again coming into contact with the workpiece slot. The smoother transitions of the measured data may also reinforce the fact that the cutting edges require several degrees of rotation to fully compress the workpiece at first contact and again to relieve the elastic compression (springback) when leaving the work.

For small radial depths of cut the signal level is small enough to require considering noise. Several passes were made with the spindle operating at speed but without contacting the work and the noise levels were recorded. For a 2 μm radial depth of cut and a 5 μm axial depth, the cutting tool completely leaves the workpiece after only 15° of rotation. With no contact, the model predicts zero forces. However, if the noise is added then the result has the same general shape as the measured data as shown in the Fig. 7. For all the data, the rms noise in the feed direction was equivalent to 6.5 mN of force and in the cross-feed direction it was 8.2 mN. At the smallest radial depth of cut, the noise tends to dominate the cutting force signal.

Using the same 100 μm diameter tool, cuts were taken with a radial depth of 2, 5, 10, 20, and 40 μm with a

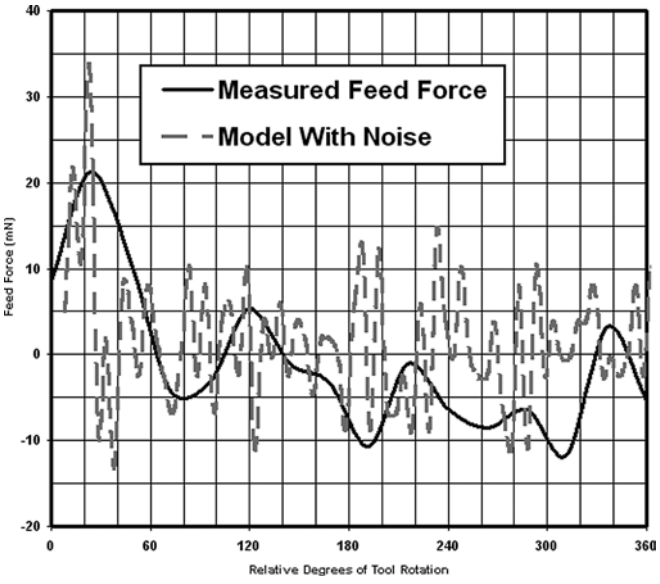

Fig. 7. Comparison of easured force in feed direction for a radial depth of cut of 2 microns and axial depth of 5 microns (solid line) and predicted force with superimposed and filtered noise (dotted line). This is the lower threshold of measured data and it is dominated by noise

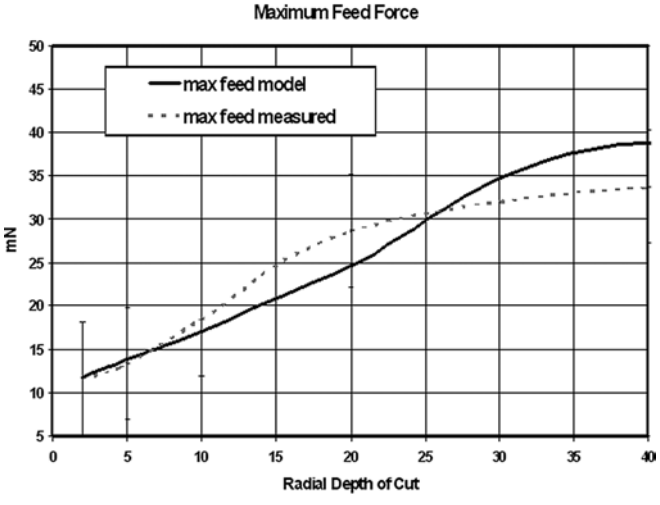

Fig. 8. Comparison of predicted (*solid*) and measured (*dotted*) force in the feed direction for 5 microns of axial depth of cut and radial depths of 2 to 40 microns with 100-micron diameter tool

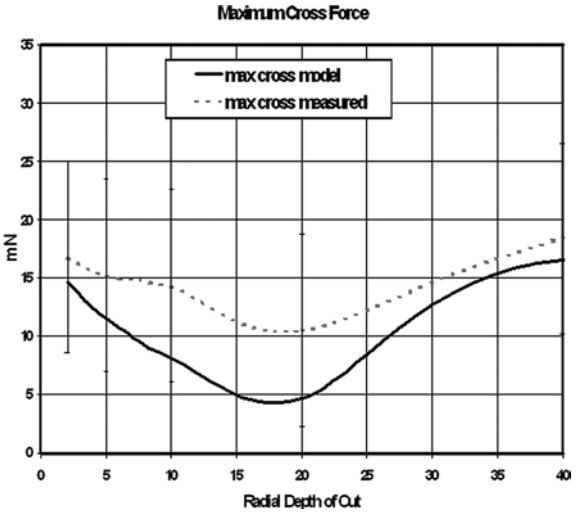

Fig. 9. Comparison of predicted (*solid*) and measured (*dotted*) force in the feed direction for 5 microns of axial depth of cut and radial depths of 2 to 40 microns with 100-micron diameter tool. Agreement in cross-feed direction is less than in feed direction due to a greater sensitivity of the force on tool geometry in this direction

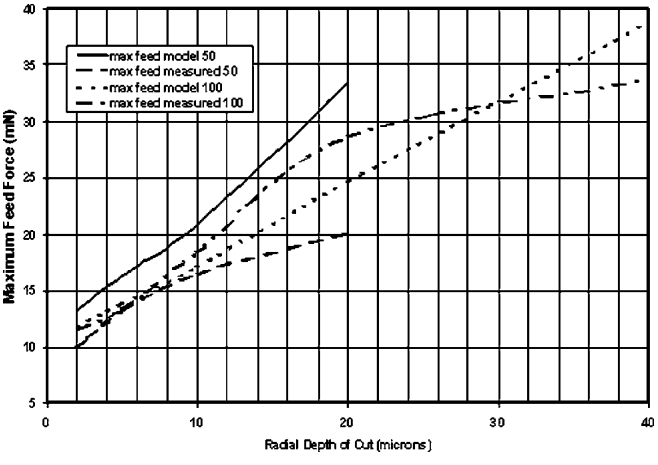

Fig. 10. Comparison of predicted and measured forces for 50- and 100-micron diameter tools with 5 micron axial depth of cut and varying radial depths. The 50-micron data extends to 20 microns radial depth and the 100-micron data extends to 40 microns radial depth. The model overpredicts the force for the 50-micron tool

constant axial depth of cut of 5 μm. The results are shown in Figs. 8 and 9. There is good agreement between the model and the experimental results in the feed direction but less agreement in the cross-feed direction. This may be due to more noise present in that direction or due to dynamic characteristics of the dynamometer in that direction.

Using a 50 μm diameter tool, the cutting tests were repeated. A comparison between the model and the measured force in the feed direction, for a typical rotation of the tool, is shown in Fig. 10, along with the prior data for the 100 μm tool. The first observation is that, whereas the 100 μm data has good agreement with the model, the data for the 50 μm tool diverges form the model in a continuous trend. This indicated that the actual forces on the 50 μm tool relative to the model predictions are less than for the 100 μm tool. This indicates the tool was probably deflecting thus reducing the magnitude of the springback and thereby reducing the magnitude of normal and friction forces on the cutting edges. It was also quickly obvious that the predicted and measured data for the 50 μm tool were significantly different for deeper trenches where multiple axial passes were used. With a tool this small it is normal to create a deep trench by taking multiple passes. The assumption was that for the second and third passes, each of 5 μm additional axial depth, the back-tapered portion of the tool above the cutting zone would experience springback due to contact with the machined

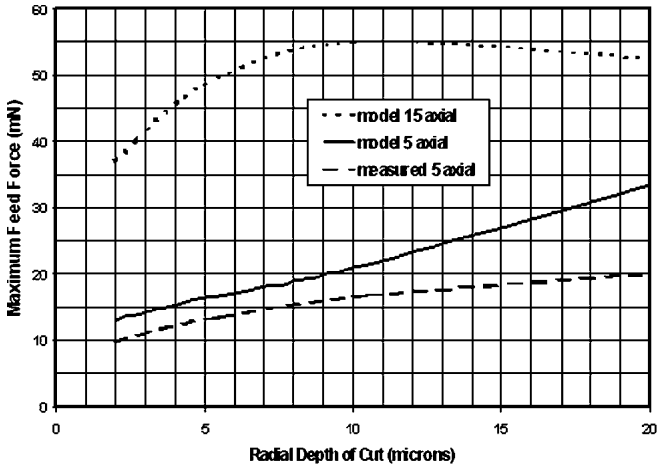

Fig. 11. Predicted force on 50-micron tool during the third 5-micron axial depth of cut for a total of 15 microns deep (upper trace) and the measured and predicted forces for a single 5-micron axial depth (2 lower traces)

wall of the previous passes. As shown in Fig. 11, this did not happen. The uppermost line is the predicted feed–direction force for a single 15 μm deep cut assuming the side cutting edge was rubbing along the vertical wall of the trench. Instead, the measured force (lowest line) closely agrees with a single 5 μm deep axial cut. The back taper angle of the tool may be sufficient to eliminate contact, and deflection of the tool may also play a role in this data. In either case, the data tends to indicate that a vertical straight wall will not result if multiple passes are used to create a deep trench. Modeling and measuring the tool deflection is beyond the scope of the present study but represents an important next step in predicting forces and the precision of micromachined parts.

References

1. **Waldorf DJ; DeVor RE; Kapoor SG** (1998) A slip-line field for ploughing during orthogonal cutting. ASME J Manufacturing Sci Eng 120: 693–698
2. **Bao WY; Tansel IN** (2000) Modeling micro-end milling operations part I: analytical cutting force model. Intl. J Machine Tools Manufacture 40: 2155–2173
3. **Bao WY; Tansel IN** (2000) Modeling micro-end milling operations part II: tool runout. Intl. J Machine Tools Manufacture 40: 2155–2192
4. **Bao WY; Tansel IN** (2000) Modeling micro-end milling operations part III: influence of tool wear. Intl. J Machine Tools Manufacture 40: 2193–2211
5. **Moriwaki T; Okuda K** (1989) Machinability of copper in ultra-precision micro diamond cutting. Annals CIRP 38(1): 115–118
6. **Furukawa Y; Moronuki N** (1988) Effect of material properties on ultra-precise cutting processes. Annals CIRP 37(1): 113–116
7. **Arcona C; Dow T** (1998) An empirical tool force model for precision machining. ASME J Manufacturing Sci Eng 120: 700–707